Shear mode bulk acoustic wave resonator based on *c*-axis oriented AlN thin film

Evgeny Milyutin,[a] Sandrine Gentil, and Paul Muralt
Ceramics Laboratory, Swiss Federal Institute of Technology (EPFL), CH-1015 Lausanne, Switzerland

(Received 19 February 2008; accepted 22 August 2008; published online 27 October 2008)

A shear mode resonator based on bulk waves trapped in *c*-axis oriented AlN thin films was fabricated, simulated, and tested. The active 1.55 μm thick AlN layer was deposited on top of an acoustic Bragg reflector composed of SiO_2/AlN $\lambda/4$ layer pairs. The resonance was excited by means of interdigitated electrodes consisting of 150 nm thick Al lines. Analytical and simulation calculations show that the in-plane electric field excites bulk acoustic wave shear modes that are trapped in such an AlN film slab. The experimental frequency corresponds well to the theoretical one. The evaluated resonance of the fundamental shear mode at 1.86 GHz revealed a coupling of 0.15% and *Q*-factor of 870 in air and 260 in silicon oil. © *2008 American Institute of Physics*. [DOI: 10.1063/1.2996319]

I. INTRODUCTION

In recent years, the rise of mobile communication has stimulated the development of thin film bulk acoustic wave resonators (TFBARs) to realize rf filters for the low gigahertz frequency range.[1,2] Such resonators are also potentially very interesting for gravimetric sensors,[3,4] which are traditionally based on AT-cut quartz plates.[5] The decrease in resonator thickness when passing from a single crystal to a thin film leads to a very marked increase in frequency. Theoretically, and also evidenced by experiments,[6] the relative frequency shift by mass loading increases linearly with frequency. The signal-to-noise ratio, however, does not increase as much. A recent comparative study showed a factor of 2 improvement of a TFBAR device as compared to a quartz microbalance device.[7] TFBARs of the type utilized in telecommunication devices are based on a longitudinal wave. The AlN or ZnO films are grown on metal electrodes and are *c*-axis oriented. The electric field is created by means of a parallel plate capacitor that points along the *c*-axis. This geometry leads to a piezoelectric stress excitation along the *c*-axis by means of the e_{33} piezoelectric coefficient. The border reflections lead to trapping of a wave running along the *c*-axis. This longitudinal mode is optimal for rf filters because the highest piezoelectric coupling is achieved in this way. The same geometry can be used for sensors operated in air.[3,4,6] However, sensors for immersed operation are more attractive because they are useful for biomedical and many environmental applications. In liquids, longitudinal waves are very much damped by acoustic emission into the liquid. For this reason it is better to use shear waves, which do not propagate in liquids.

Many efforts have recently been made to grow AlN and ZnO thin films whose *c*-axis is tilted with respect to the film normal.[8–11] In this way, the shear coupling through the e_{15} piezoelectric coefficient comes into play in parallel plate capacitors and a mixed, shear, and longitudinal excitation is achieved. The fact that the shear wave exhibits a much lower sound velocity than the longitudinal wave allows for trapping the shear mode selectively, thus suppressing the longitudinal mode to a large extent. The disadvantages of this method are associated with achieving a homogeneous *c*-axis tilt across the wafer. The design of the magnetron source for homogeneous tilting is not evident and certainly does not correspond to a standard tool as currently optimized by industry, which by now achieves impressive results in terms of uniformity of thickness and piezoelectric coupling of *c*-axis oriented AlN.

In this work, we investigate another solution. It is sought to use standard AlN thin films that are useful for rf filters, but instead we tilt the electric field into the plane of the film by using interdigitated electrodes (IDEs). We will first show that a BAW mode of shear symmetry can indeed be generated in this way. Important requirements for the realization of such a structure are: growth of good piezoelectric thin films on an insulator such as a SiO_2 layer and a design that avoids mixing of the desired shear bulk mode with Rayleigh, Love, or Lamb waves. We do not use a membrane structure but employ an acoustic reflector to suppress emission into the substrate. This eliminates the occurrence of Lamb waves. Attempts to create such resonators based on ZnO were very recently published by Corso *et al.*[12] A *Q*-factor of about 550 in air and the capability of operating in liquid were reported without, however, showing details for the latter. These authors employed a reflector based on W layers, which short circuit the electric field, leading to strong vertical components of the electric field below the electrodes, and only weak horizontal fields in between the two electrodes. According to their simulations, the active layer operates not in a shear mode but in some other mode type, probably due to transverse strain in the film plane (e_{31} coefficient). In our work we use a pure dielectric reflector stack AlN/SiO_2, which leads to an electric field that is mainly along the *x*-axis in the plane of the film. In addition, we extended the two electrodes to a larger IDE system.

[a]Electronic mail: evgeny.milyutin@epfl.ch.

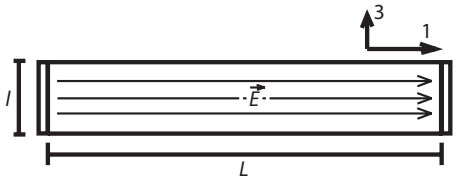

FIG. 1. Thin film of AlN with in-plane electric field inside (ideal situation).

II. THEORETICAL BACKGROUND

A. Concept

The shear mode sought requires the exciting electric field to be perpendicular to the propagation direction. This is a major difference in the traditional longitudinal TFBAR. For this reason the major derivation steps are presented in this section to show that the existence of this mode also follows from simple analytical modeling (our approach differs to that of Corso *et al.*[12]). For an AlN plate with its *c*-axis oriented perpendicular to plane, Newton's wave equation is combined with Maxwell's equations including the electromechanical coupling,

$$\rho \ddot{u}_i = \frac{\partial T_{ij}}{\partial x_j}, \tag{1}$$

$$T_{ij} = c^E_{ijkl} S_{kl} - e_{nij} E_n, \tag{2}$$

$$D_n = \epsilon_{nj} E_j + e_{nkl} S_{kl}, \tag{3}$$

$$\text{rot}\, \vec{E} = 0, \quad \text{div}\, \vec{D} = 0, \tag{4}$$

where u_i, T_{ij}, S_{ij}, E_j, and D_n are mechanical displacement field, stress and strain tensors, electric field intensity, and electric displacement filed, respectively.

As usual, the upper index in c^E_{ijkl} denotes the condition at constant electric field. In the following, we will use reduced index notation, and understand c_{ij} to be for constant field. In the applied coordinate system, direction 3 points perpendicular to the film plane and is at the same time the sixfold polar axis of the AlN single crystal grain and the long growth direction of the grain. The overall symmetry of the polycrystalline textured film is cylindrical, and results in the same matrix symmetry as for single crystal AlN.

For an electric field pointing along the x_1 direction (Fig. 1), Eq. (2) becomes

$$T_i = c_{ij} S_j, \tag{5}$$

where $i,j = 1,2,3,4,6$ and

$$T_5 = c_{55} S_5 - e_{15} E_1. \tag{6}$$

We can see that only the S_5 strain of the film is coupled with the electric field E_1 and that this deformation is not coupled with any other deformation. Hence the excited wave contains only displacements corresponding to S_5.

For a clamped thin film, S_5 is equal to $\partial u_1 / \partial x_3$. Introducing the Maxwell equations, it follows that all variables depend on x_3 only. Then by solving Maxwell's equations and Newton's equation together with the equations of electromechanical coupling, we obtain

$$\frac{\partial E_1}{\partial x_3} = 0, \quad \frac{\partial E_1}{\partial x_1} = 0, \tag{7}$$

$$\rho \ddot{u}_1 = \frac{\partial T_5}{\partial x_3}, \tag{8}$$

$$\frac{\partial T_5}{\partial x_3} = c_{55} \frac{\partial S_5}{\partial x_3} = c_{55} \frac{\partial^2 u_1}{\partial x_3^2}. \tag{9}$$

So,

$$\rho \ddot{u}_1 = c_{55} \frac{\partial^2 u_1}{\partial x_3^2}. \tag{10}$$

The last equation describes shear waves that propagate in the x_3 direction [wave vector $(0, 0, k_3)$] and with displacement in the x_1 direction. The current and the voltage between electrodes can easily be derived and admittance $Y = I/U$ is finally equal to

$$Y = j\omega C_0 \left(1 + \frac{e_{15}^2}{c_{55}\epsilon_{11}} \frac{\tan(\varphi)}{\varphi} \right), \quad \varphi = \frac{k_3 l}{2}, \tag{11}$$

where C_0 is the static capacitance between the electrodes and wave number $k_3 = \omega\sqrt{\rho / c_{55}}$. Resonances are observed for infinite values of $\tan(\varphi)$. At the antiresonance frequency the admittance becomes zero. The difference between the resonance and antiresonance frequencies is proportional to the piezoelectric coupling constant $e_{15}^2 / c_{55}\epsilon_{11}$. Note that the value of e_{15} does not affect the resonance frequency but strongly affects the antiresonance frequency. This is the result of the fact that c_{55} at constant *E*-field is relevant for the wave propagation, as follows from Maxwell's Eq. (4). Our result contradicts the theory presented by Corso *et al.*[12] in which the wave number is derived as c^D dependent.

B. Field element modeling

As a first task infinite element method (FEM) simulation, we confirmed our theoretical results. An in-plane ac electric field is produced in a slab of AlN(001), as in Fig. 1, allowing motions in the field direction (index 1) only. The resulting displacements at resonance are exactly those expected of a pure shear mode (Fig. 2). The resonance frequency was found to obey exactly Eq. (11) of the analytical $1-d$ model. The coefficient e_{15} was varied from one to three times the literature value of $-0.48(C/m^2)$ for AlN. The dependence of resonance and antiresonance frequencies are depicted in Fig. 2, showing that the behavior of the analytical model is exactly reproduced.

In practice, it is difficult to create a pure in-plane electric field, because it would require very precise patterning of the active AlN film without avoiding completely stray fields. A more practical way of supplying in-plane electric fields is the use of IDEs. In this geometry, the electric field has opposite directions in neighboring IDE sections leading to an antiphase motion in adjacent regions. This will lead to some perturbation from the ideal case. For this reason, FEM modeling has been carried out to quantify the details of the resulting motion. The silicon substrate was included using the boundary element method (BEM). Apart from the regions of

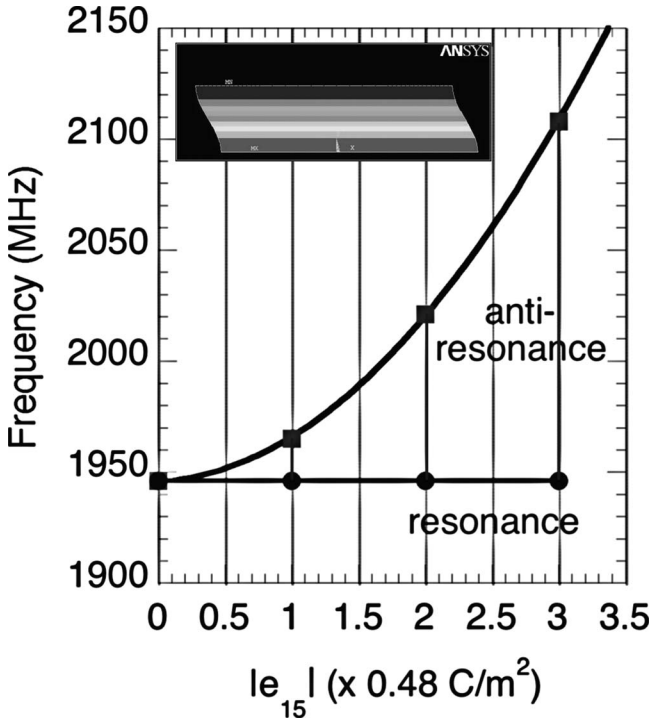

FIG. 2. Resonance and antiresonance frequencies as a function of the piezoelectric coefficient e_{15}, as obtained from FEM simulation. The insert shows the motion shape, i.e., the u_1 displacement intensity in a contour plot.

electrodes, FEM-BEM modeling shows that the electric fields of the IDEs lead to an excitation that is close to the ideal one, as used for the analytical calculation.

The properties of the solidly mounted resonator with a periodic planar electrode system were simulated with the help of ANSYS and the FEM-BEM coupling module from Microsonics. A half-period of the mechanical response at resonance frequency is shown in Fig. 3. The electrode is located in the center on the top of the structure, the bottom border is clamped to a semi-infinite substrate, and half-period conditions are established along the horizontal axis.

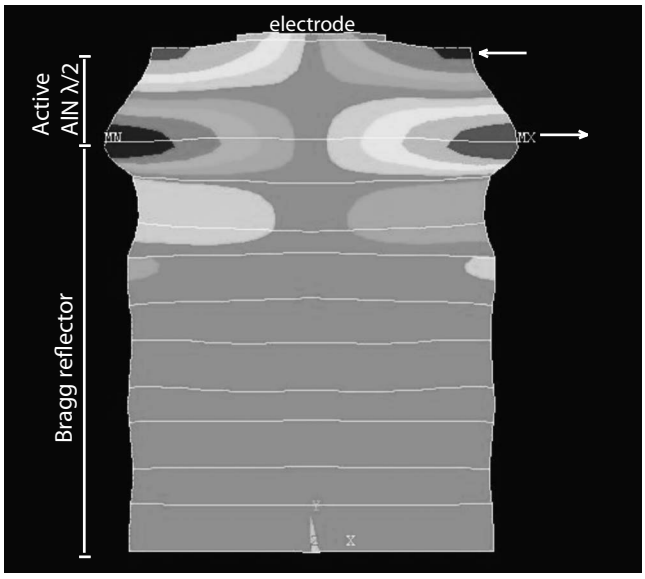

FIG. 3. FEM-BEM simulation: motion of the device at resonance frequency.

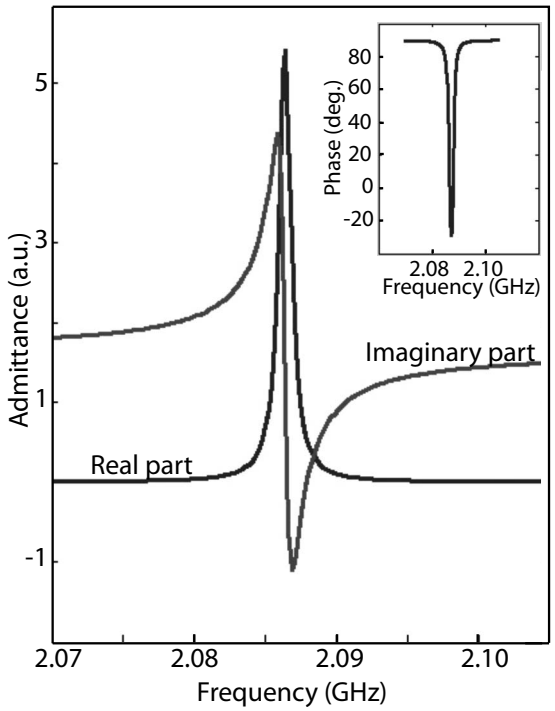

FIG. 4. FEM-BEM simulation: simulated admittance curve of the device.

The fact that we are dealing with shear waves can easily be ascertained from the type of resonant motion within the active AlN layer.

It is important to emphasize several peculiarities as follows. (1) A shear mode thickness resonance can be seen between the electrodes (at the left and right of the center of the structure). (2) The most intense motion is concentrated in the top layer of AlN and the amplitude decreases strongly within the Bragg reflector. (3) The displacement of the AlN surface between electrodes is mostly horizontal, which is very important for sensors in liquid applications. (4) There are small vertical displacements of the electrode, which are expected to contribute to losses in immersed operation. The simulated electrical admittance is shown in Fig. 4, from which a Q-factor of 2000 and coupling coefficient of 0.2% are derived.

The material constants used for AlN are given in Table I (from Ref. 13). The following material constants for SiO_2 were also used: density of 2200 kg/m^3, Poisson's ratio of 0.171, and Young's modulus of 70 GPa. Electrical resistivity of electrodes and mechanical losses of materials were not taken into account. The finite quality factor of the resonance results entirely from the acoustic emission into the substrate through the Bragg grating. The thickness of the electrode has only a minor effect on the resonance frequency. The latter was found to be 2086 and 2074 MHz for 100 and 150 nm thickness, respectively.

III. FABRICATION

A top view and a cross-sectional view of a typical device are shown in Figs. 5 and 6. The device consists of a reflector composed of five pairs of SiO_2 and AlN layers (similar as in Ref. 14). Such reflectors were originally proposed and fabricated by Lakin *et al.*[2] for rf filters based on the longitudinal

TABLE I. Properties of AlN used in FEM-BEM simulation.

Stiffness constants (GPa)				Piezoelectric coefficient (pm/V)			Density (kg/m^3)
c_{11}^E	c_{12}^E	c_{13}^E	c_{55}^E	d_{31}	d_{33}	d_{15}	ρ
345	125	120	118	−2.64	5.53	−4.07	3260

mode. They require more layers than the commonly used SiO_2/W type, but have the advantage of being electrically insulating. As explained earlier, this is extremely important for the IDE shear mode excitation. The critical issue in reflector stack deposition is the stress control to avoid accumulation of bending moments, as described in an earlier work of the EPFL group,[15,16] and later by the CSEM group.[17] We deposited the AlN thin films by pulsed dc reactive magnetron sputtering[18,19] and the SiO_2 films by rf sputtering at a temperature of 300 °C. The stress within AlN films can be adjusted more easily than that within SiO_2. For this reason, the AlN process was optimized to compensate the SiO_2 film stress of −200 MPa. The active $\lambda/2$ AlN layer is deposited on the top SiO_2 layer of the reflector. A very thin layer of SiO_2 on top of the active AlN layer was used to protect the AlN from being attacked by the developer solution during subsequent photolithography for aluminum electrode patterning. The 150 nm thick aluminum electrodes with chromium adhesion layers were evaporated at room temperature, and patterned by means of a lift-off process using a double layer resist (lift-off resist (LOR)+AZ1512 photo resist). This device thus needs only one photolithography step, and not two as the simplest possible TFBAR.

All devices were designed to have equal static capacitance, but at the same time the distance between the centers of neighboring electrode fingers was varied from 6 to 10 μm in order to test the resonance frequency dependence on the IDE dimensions. In case of a pure shear thickness mode excitation no such dependence must be observed.

IV. EXPERIMENTAL RESULTS AND DISCUSSION

The performance of the resonators was assessed using a Cascade Microtech probe and HP Network analyzer in air and in silicon oil [Poly(dimethylsiloxane), viscosity of 0.65 cS]. Typically, the resonance frequency of devices operated in air was between 1.8 and1.9 GHz, depending on the position on the wafer. This effect is due to a nonuniform AlN film thickness. The resonance frequency was found to change very weakly with increasing distance between adjacent finger electrodes. The change amounted to less than 2% when the distance between the fingers was almost doubled, from 6 to 10 μm (Fig. 7). The devices for this study were built near each other on the wafer, thus having equal thickness of all layers (active layer: 1.55 μm). The thickness mode nature of the resonance is thus confirmed, excluding any wave dependent on IDE periodicity. The small change in frequency with short electrode distance must be assigned to the stronger admixture of up and down motions below the center of the electrode, leading to a stiffening.

The sensitivity of the sensor depends crucially on the width of the resonance curve, because the shift of the resonance curve is more precisely measured when the resonance peak is narrower. This width is inversely proportional to the quality factor Q, which is evaluated as the ratio between full width at half maximum of the conductance peak, as a function of frequency to the resonance frequency. The maximum Q-factor was thus determined to be 870 in air (Fig. 8). This Q-factor is smaller than the simulated one, since the latter did not take into account material losses.

The coupling coefficient (k^2) amounted to 0.15% in this case, which is in agreement with simulations. As compared to FEM and analytical calculations, the experimental resonance frequencies turned out to be around 10% lower. It is possible that the shear stiffness of a columnar microstructure is smaller than that of an epitaxial film, as investigated by Tsubouchi *et al.*,[13] whose value of $c_{55}=118$ GPa was applied in FEM-BEM simulations.

The conductance curve of the device immersed in silicon oil is shown in Fig. 9. The peak amplitude is decreased as well as the Q-factor and a small shift of the resonance frequency (2 MHz) takes place. This shift may have two pos-

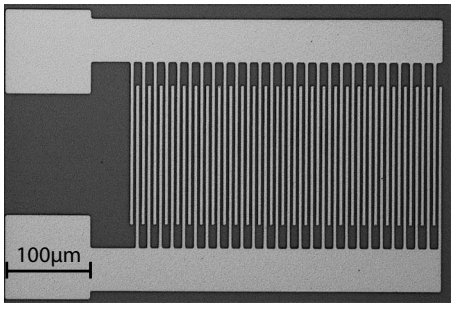

FIG. 5. Top view image of the typical resonator fabricated in this work.

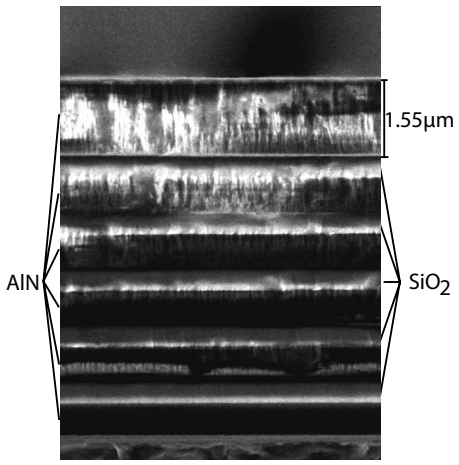

FIG. 6. Cross-sectional scanning electron microscopy image of typical resonator fabricated in this work.

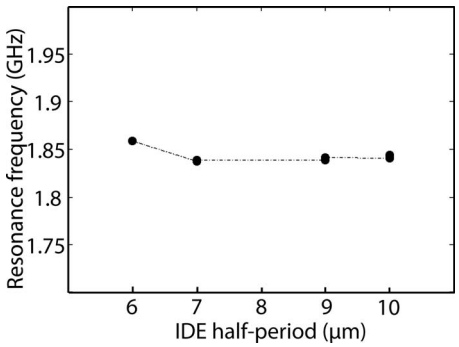

FIG. 7. Changes in resonance frequency vs IDE period.

sible origins. The first one can be a loading effect due to the local piston motion of the electrode regions, which contain the previously discussed longitudinal (i.e., vertical) wave component. As a second origin we can see surface roughness or asperities. As the liquid has some finite viscosity, it is dragged to a certain depth, and thus the shear wave is loaded as well. The Q-factor measured in immersed operation amounted to 260. According to our simulation calculations comparing the actual resonator with an ideal homogeneous shear resonator, the additional damping is mostly due to the piston movement in the electrode finger regions. However, the achieved Q-factor in the liquid is still high enough for sensor applications. In comparison, Wingqvist *et al.*[9] reported a Q-factor of 150 achieved by a shear mode thin film bulk acoustic resonator based on inclined c-axis AlN, operated at a lower frequency of 1.2 GHz.

In the future, the device will be completed as a sensor. It will be covered by a SiO_2 layer, on top of which an organic immobilization layer will be grafted. The resonant frequency is expected to shift when the surface mass density, or stiffness of this layer, changes upon adsorption of or reaction with organic molecules from the liquid (mostly water). The immobilization layer may contain, for instance, antigenes that attach the corresponding antibodies.

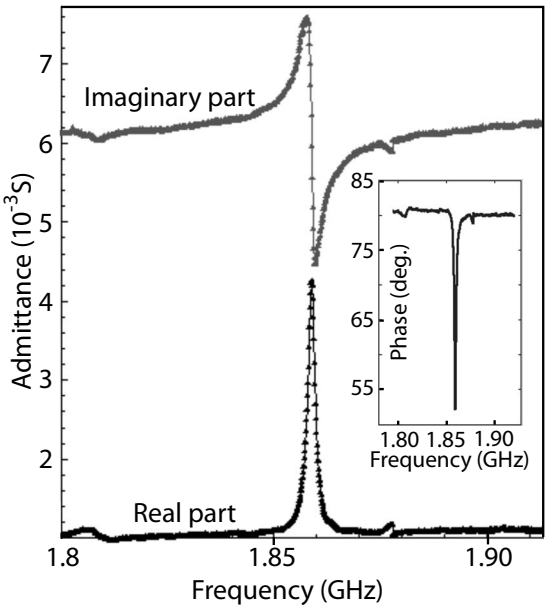

FIG. 8. Measured admittance curve (real and imaginary parts) for a device with an IDE period of 6 μm and a finger width of 3 μm.

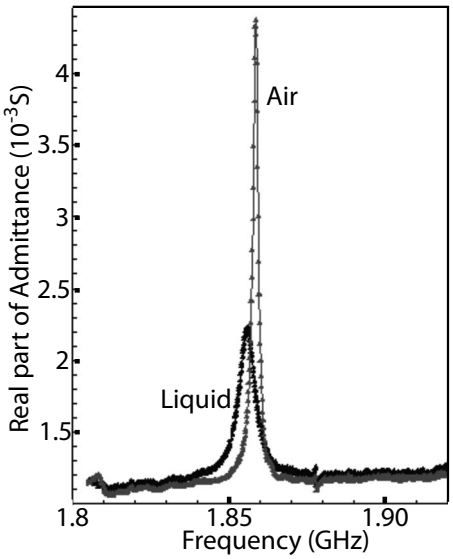

FIG. 9. Real part of admittance curve for the device operated in air and silicon oil.

V. CONCLUSIONS

We have shown by a simple one-dimensional model that standing shear bulk acoustic waves can be excited in a piezoelectric slab with an in-plane electric ac field. In contrast to the well-known longitudinal bulk acoustic waves, their resonance frequency depends on the stiffness at constant E-field and not at constant D-field. The FEM simulation was extended to a full two-dimensional simulation model for a realizable device based on IDEs, including an acoustic reflector. A specific boundary element method was applied to deal with the boundary condition underneath the reflector. The model confirmed that IDEs excite mainly the desired shear mode, however, with a deviation from the ideal motion below the electrodes. We succeeded in the fabrication of test devices that show resonance frequencies close to the calculated ones, and that vary only slightly with the electrode spacing, as expected for such modes. Importantly for sensors, the immersion into a low-viscosity siloxane liquid still allowed for a high Q-factor of 260, and only slightly shifted the resonance frequency. The results achieved and the simplicity of the fabrication of such devices show their potential as gravimetric sensors for biomedical and environmental applications.

ACKNOWLEDGMENTS

The support of the Swiss National Science Foundation (Contract No. 20021-112204) and the Swiss Center of Competence on Materials is gratefully acknowledged. The device fabrication was carried out in the central micromachining facility of EPFL.

[1] R. C. Ruby, P. Bradley, Y. Oshmyansky, A. Chien, and J. D. Larson, Proceedings of the IEEE Ultrasonics Symposium (IEEE, Atlanta, 2001).
[2] K. M. Lakin, K. T. McCarron, and R. E. Rose, Proceedings of the IEEE Ultrasonics Symposium, Seattle, WA (IEEE, Washington, 1995).
[3] R. Gabl, H.-D. Feucht, H. Zeininger, G. Eckstein, M. Schreiter, R. Primig, D. Pitzer, and W. Wersing, Biosens. Bioelectron. **19**, 615 (2004).
[4] M. Benetti, D. Cannata, F. Di Pietrantionio, V. Foglietti, and E. Verana, Appl. Phys. Lett. **87**, 173504 (2005).

[5]E. Gizeli, in *Biomolecular Sensors*, edited by E. Gizeli and C. R. Lowe (Taylor & Francis, London, 2002).
[6]S. Rey-Mermet, R. Lanz, and P. Muralt, Sens. Actuators B **114**, 681 (2006).
[7]J. Weber, W. M. Albers, J. Tuppurainen, M. Link, R. Gabl, W. Wersing, and M. Schreiter, Sens. Actuators, A **A128**, 84 (2006).
[8]J. Bjurstrom, G. Wingqvist, and I. Katardjiev, IEEE Trans. Ultrason. Ferroelectr. Freq. Control **53**, 2095 (2006).
[9]G. Wingqvist, J. Bjurstrom, L. Liljeholm, V. Yantchev, and I. Katardjiev, Sens. Actuators B **123**, 466 (2007).
[10]T. Yanagitani, M. Kiuchi, M. Matsukawa, and Y. Watanabe, IEEE Trans. Ultrason. Ferroelectr. Freq. Control **54**, 1680 (2007).
[11]T. Yanagitani, M. Kiuchi, M. Matsukawa, and Y. Watanabe, J. Appl. Phys. **102**, 024110 (2007).
[12]C. D. Corso, A. Dickherber, and W. D. Hunt, J. Appl. Phys. **101**, 054514 (2007).
[13]K. Tsubouchi, K. Sugai, and N. Mikoshiba, in Proceedings of the 1981 Ultrasonics Symposium, edited by B. R. McAvoy (IEEE, New York, 1981). Vol. 1, p. 375.
[14]R. Lanz and P. Muralt, IEEE Trans. Ultrason. Ferroelectr. Freq. Control **52**, 936 (2005).
[15]M.-A. Dubois, P. Muralt, and V. Plessky, Proceedings of the IEEE Ultrasonics Symposium, Lake Tahoe, 1999, Vol. 2, pp. 907–910.
[16]M.-A. Dubois, P. Muralt, H. Matsumoto, and V. Plessky, Proceedings of the IEEE Ultrasonics Symposium, Sendai, Japan, 1998, pp. 909–912.
[17]M.-A. Dubois, Proceedings of the MEMSWAVE, Toulouse, 2003 (unpublished).
[18]M.-A. Dubois and P. Muralt, Appl. Phys. Lett. **74**, 3032 (1999).
[19]M.-A. Dubois and P. Muralt, J. Appl. Phys. **89**, 6389 (2001).